Fate of an Impurity Strongly Interacting with a Thermal Bose Gas

Jiří Etrych,[1] Sebastian J. Morris,[1] Simon M. Fischer,[1] Gevorg Martirosyan,[1] Christopher J. Ho,[1] Moritz Drescher,[2] Manfred Salmhofer,[2] Zoran Hadzibabic,[1] Tilman Enss,[2] and Christoph Eigen[1,*]

[1]*Cavendish Laboratory, University of Cambridge, J. J. Thomson Avenue, Cambridge CB3 0HE, United Kingdom*

[2]*Institut für Theoretische Physik, Universität Heidelberg, 69120 Heidelberg, Germany*

(Received 2 September 2025; revised 24 June 2026; accepted 28 September 2026; published 5 November 2026)

We spectroscopically study mobile impurities immersed in a homogeneous bosonic bath (a box-trapped Bose gas), varying the bath temperature and the strength of impurity-bath interactions. We compare our results to those for a quasipure Bose-Einstein condensate, and find that for strong impurity-bath interactions, the spectra narrow with increasing temperature, while the impurity energy shift is suppressed. Near the critical temperature for condensation, many-body effects still play an important role, and only for a nondegenerate bath the system approaches the classical Boltzmann-gas behavior. The key spectral features are reproduced within the theory of the ideal Bose polaron.

DOI: 10.1103/g8gh-vsyq

An impurity immersed in a quantum bath is a fundamental setting in many-body physics that, in spite of its apparent simplicity, features complex emergent behavior. A key simplification often lies in treating the impurities dressed by the excitations of the bath as polaron quasiparticles. This notion originates from descriptions of electrons moving through a polarizable crystal [1,2], but nowadays extends to numerous scenarios in condensed matter physics and beyond [3,4].

In cold-atom experiments, impurity physics can be studied in highly imbalanced two-component mixtures, where the minority component acts as impurities and the majority component as the bath [5–8]. A key advantage of these experiments is the high degree of tunability: the bath density n and temperature T are readily controllable, and the strength and sign of the impurity-bath interactions, characterized by the s-wave scattering length a, can be tuned using Feshbach resonances. In the high-temperature regime, the mixture can be described as a classical Boltzmann gas, and the thermal de Broglie wavelength $\lambda \propto 1/\sqrt{T}$ sets the relevant interaction parameter a/λ. Instead, in the low-temperature regime, the impurity behavior depends on the quantum statistics of the bath, and is generally governed by the interaction parameter $k_n a$, where $k_n = (6\pi^2 n)^{1/3}$ [5–8].

For a fermionic bath, long-lived attractive and repulsive polaron quasiparticles exist for temperatures well below the Fermi temperature [9,10], but the quasiparticle description breaks down as T is increased [11]. The situation is more intricate for a bosonic bath: in the limit of vanishing intrabath interactions ($k_n a_b \to 0$, where a_b is the intrabath scattering length), there is no overlap between the ground state of the system with and without the impurity; this is known as the bosonic orthogonality catastrophe [12,13]. When the bath is weakly repulsive and the reduced temperature $T/T_c \ll 1$, where T_c is the critical temperature for Bose-Einstein condensation, well-defined attractive and repulsive polarons exist at sufficiently low $|a|$ [14–19], but in the strongly interacting regime the quasiparticle picture breaks down and the spectra are intrinsically broad [19]. The fate of the system at nonzero T, including the effect of the condensation phase transition, is subject to ongoing theoretical debate [20–26], with previous experiments limited to strong attractive interactions [27]. Furthermore, in contrast to fermions, strongly interacting bosons are unstable due to three-body loss (owing to the absence of Pauli blocking), making it challenging to investigate their equilibrium properties.

In this Letter, we study impurities injected into a box-trapped Bose gas, mapping out the impurity spectrum across the strong-coupling regime for different T/T_c. We compare our measurements to those obtained for a quasipure Bose-Einstein condensate (BEC) [19], and find that the spectral shift in a thermal gas is suppressed compared to the BEC and, counterintuitively, near unitarity the spectra narrow with increasing T. Near T_c, the spectra retain clear many-body character, with three key signatures: (i) the spectral shifts and widths are set by the energy scale $E_n = \hbar^2 k_n^2/(4m_r)$, where m_r is the reduced mass of an impurity and a bath atom (in our equal-mass case $m_r = m/2$, where m is the atom mass), (ii) the attractive branch extends across the resonance, and (iii) the spectral

*Contact author: ce330@cam.ac.uk

Published by the American Physical Society under the terms of the Creative Commons Attribution 4.0 International license. Further distribution of this work must maintain attribution to the author(s) and the published article's title, journal citation, and DOI.

width is asymmetric in $1/(k_n a)$, reaching a maximum value for $1/(k_n a) \approx 0.4$. For higher T/T_c, the system approaches the Boltzmann-gas regime: the attractive and repulsive spectral branches connect across the resonance, and the width is symmetric in λ/a, reaching its maximum (unitarity-limited) value at $\lambda/a \approx 0$. Throughout, we compare our results to bosonic functional determinant approach (FDA) calculations for the ideal Bose polaron [26,28] (see also Refs. [23,29]), finding good qualitative agreement.

Our experiments are performed using a gas of ^{39}K atoms in an optical box trap [30–32] of volume $V = 3.3(7) \times 10^4$ μm^3, initially spin polarized in the $|F, m_F\rangle = |1, -1\rangle$ state, here denoted as $|\uparrow\rangle$. We prepare thermal samples with T/T_c up to ≈4, varying both the temperature and the density of the sample [33]. As illustrated in Fig. 1(a) and following Ref. [19], we perform rf injection spectroscopy by coupling $|\uparrow\rangle$ to the $|1, 0\rangle = |\downarrow\rangle$ (impurity) state with long, weak pulses [34] of frequency $\omega/(2\pi)$, and measure the fraction of atoms transferred to $|\downarrow\rangle$ as a function of the detuning $\delta/(2\pi)$ from the bare atomic transition frequency $\omega_0/(2\pi)$, such that $\omega = \omega_0 + \delta$. We tune the impurity-bath interactions by changing the magnetic field in the proximity of the interstate Feshbach resonance at $B_{res} = 526.16(3)$ G [19]; the intrabath interactions are always weakly repulsive, with the intrastate ($|\uparrow\rangle$–$|\uparrow\rangle$) scattering length $a_b \approx 20 a_0$.

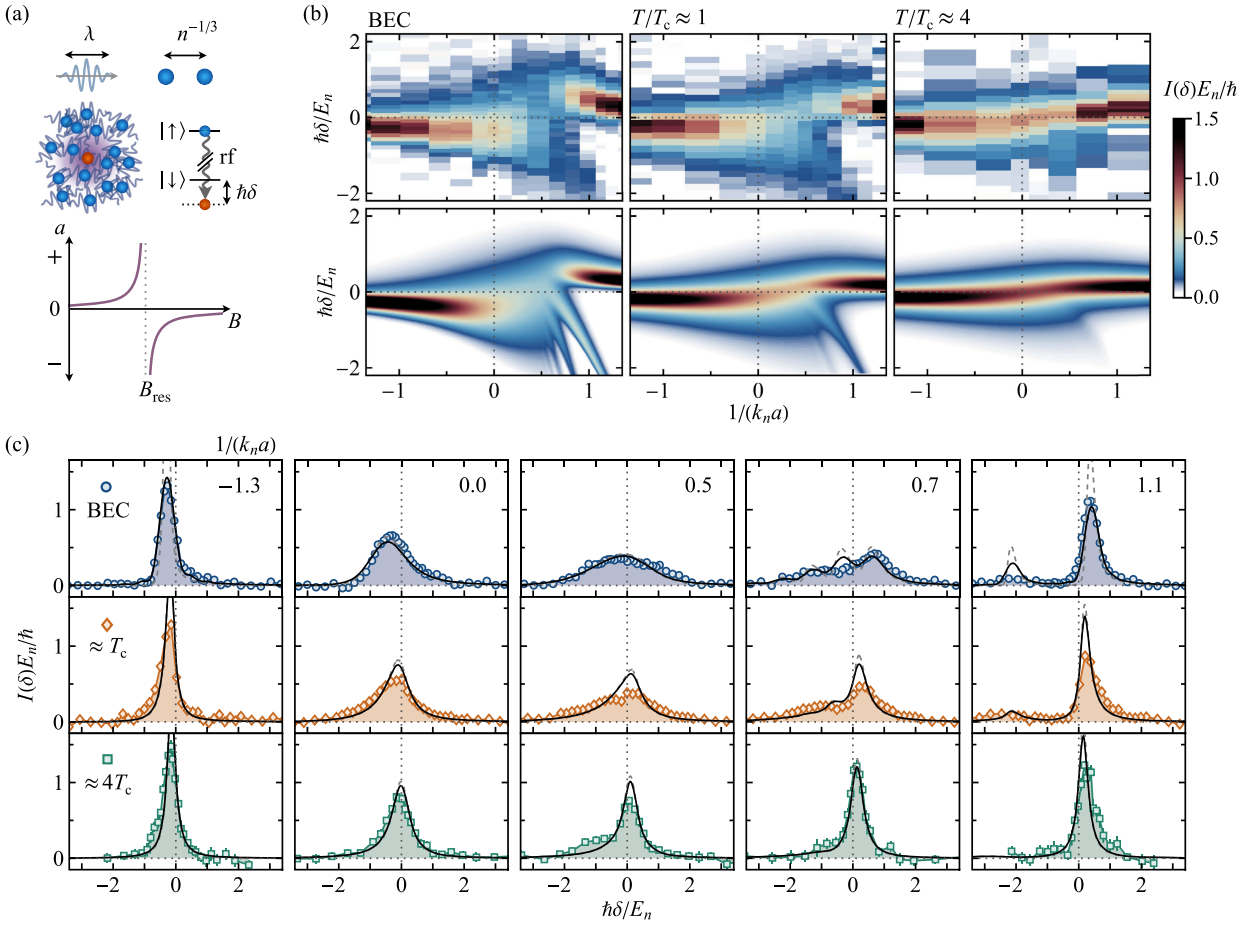


FIG. 1. Injection spectroscopy of impurities in a bosonic bath. (a) We start with a spin-polarized Bose gas, with tunable thermal wavelength $\lambda \propto 1/\sqrt{T}$ and interparticle separation $n^{-1/3} \propto 1/k_n$, set by the gas temperature T and density n (top). We use rf pulses of variable detuning δ to inject a small fraction of impurities, mapping out the spectral response $I(\delta)$ (middle). The impurity-bath interactions, characterized by the interstate scattering length a, are tunable by changing the magnetic field B in the vicinity of a Feshbach resonance (bottom). (b) Experimental impurity spectra (top) and ideal-polaron calculations (bottom) in the strong-coupling regime for three different baths: an initially quasipure Bose-Einstein condensate (BEC) with $n \approx 12$ μm^{-3} [19] (left), a Bose gas near the critical temperature for condensation T_c [$T \approx 130$ nK, $n \approx 5$ μm^{-3}] (middle), and a thermal gas at $T/T_c \approx 4$ [$T \approx 260$ nK, $n \approx 1.7$ μm^{-3}] (right). (c) Example experimental (symbols) and theoretical (solid lines) injection spectra for our three bath temperatures at different $1/(k_n a)$ (left to right), corresponding to vertical cuts through the panels in (b). In the strong-coupling regime, the spectral response narrows with increasing T. Note that we have convolved the theoretical spectra with the residual Fourier broadening (arising from the finite rf-pulse duration); for comparison, the dashed lines (in most cases indistinguishable from the solid lines) show the unconvolved spectra.

To measure the injected impurity population, at the end of each experimental sequence we quench $B \to B_{\mathrm{res}}$ and wait for all impurities to be lost, recording the total loss fraction $\Delta N/N$.

The theoretical spectra are calculated within the FDA for the ideal Bose polaron, a stationary (infinite-mass) impurity in a noninteracting Bose gas (see Ref. [26] and Appendix A for further details on the calculations). The calculations are exact for this limit and include an arbitrary number of excitations of the bath (capturing macroscopic deformations of it), but the model itself applies only approximately to our experiment; in particular, it neglects short-range bath correlations due to intrabath repulsion and/or three-body physics, and it naturally cannot capture impurity motion (which also induces bath correlations). To compare to this theory, we set m_{r} to our value $m/2$.

In Fig. 1(b), we show an overview of our main results, the injection spectra $I(\delta)$ in both experiment (top) and theory (bottom), for various $1/(k_n a)$ and three different baths: an initially quasipure BEC ($T/T_{\mathrm{c}} < 0.1$), a Bose gas near criticality ($T/T_{\mathrm{c}} \approx 1$) [35], and a thermal gas ($T/T_{\mathrm{c}} \approx 4$) [35]; the spectra are normalized such that $\int I(\delta)\mathrm{d}\delta = 1$ and for the BEC comparison, we use $T/T_{\mathrm{c}} = 0.15$ in the theory (see Appendix B). For the BEC case, the attractive branch extends to $1/(k_n a) > 0$ and for $1/(k_n a) > 0.5$, both the attractive ($\delta < 0$) and the repulsive ($\delta > 0$) branches are clearly resolved. For $T/T_{\mathrm{c}} \approx 1$, the spectral shifts are generally suppressed compared to the BEC case. Across the resonance, spectral weight is more continuously transferred between the two branches, but the attractive branch still extends to $1/(k_n a) > 0.5$. For $T/T_{\mathrm{c}} \approx 4$, the spectral shift near unitarity is fully suppressed, the two branches connect across the resonance, and there is little attractive-branch spectral weight for $1/(k_n a) > 0$.

The ideal-polaron calculations reproduce the qualitative features of the experimental spectral functions, with the exception of the attractive branch at $1/(k_n a) > 0.5$, where the theory predicts multiple well-separated peaks, while a single broad feature is observed in the experiment. In the theory, the multiple peaks correspond to the impurity binding with multiple bath atoms, with binding energies that are integer multiples of the single-boson binding energy (see also Ref. [36]). However, this behavior is known to be pathological; for mobile impurities and realistic intrabath interactions, the short-range bath correlations are expected to break the simple integer scaling and suppress the weight of the lower-lying states [37]. The inclusion of these effects would likely improve the agreement with the experiment, but a quantitative understanding of these states remains a challenge [19] (see also Refs. [38,39]).

In Fig. 1(c), we show example spectra for our three T/T_{c} at different $1/(k_n a)$. The temperature effects are the most striking in the range $0 \lesssim 1/(k_n a) \lesssim 0.7$, where the BEC spectra are the broadest. For $T/T_{\mathrm{c}} \approx 1$, the widths of the spectra are comparable to or smaller than for the BEC, and for $T/T_{\mathrm{c}} \approx 4$ the spectra are significantly more narrow. This behavior is notably different from the temperature evolution of spectral features in cold Fermi gases, where broadening with increasing temperature is generally observed, and only at temperatures above the Fermi temperature the spectra slowly narrow as $1/\sqrt{T}$ due to unitarity-limited collisions [11,40].

We characterize the spectra by their peak position E_{p}/E_n and half-width-at-half-maximum $\hbar\Gamma/E_n$ [41], and in Fig. 2, we plot these extracted quantities as a function of $1/(k_n a)$. For $T/T_{\mathrm{c}} \approx 1$, the measured $|E_{\mathrm{p}}|/E_n$ values are significantly lower than for the BEC, but they change only slowly

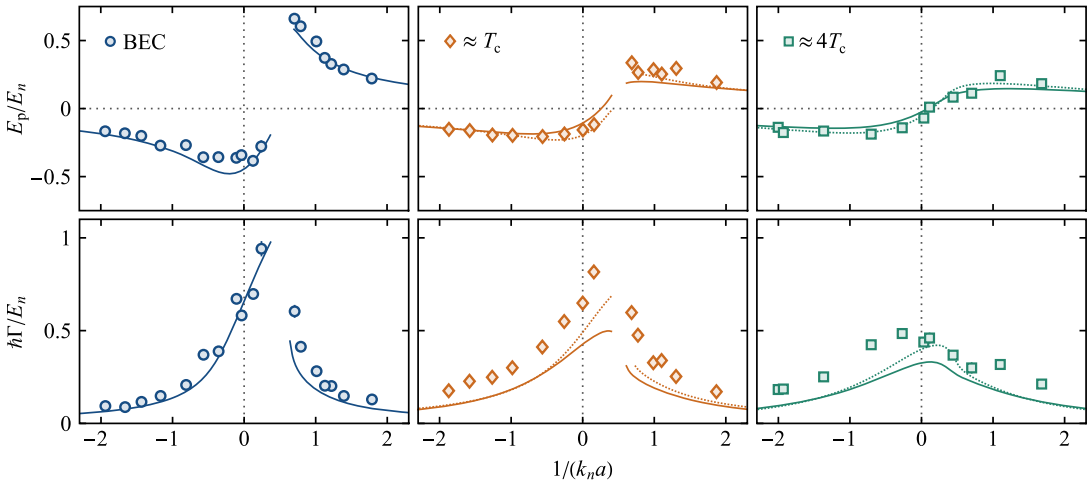


FIG. 2. Spectrum mode E_{p}/E_n (top) and half-width-at-half-maximum $\hbar\Gamma/E_n$ (bottom) versus $1/(k_n a)$ for our three different baths (increasing T/T_{c} left to right); the solid lines show the corresponding ideal-polaron FDA calculations. The dotted lines show ideal-polaron FDA calculations at half the bath temperature, so that T/E_n is the same as in the experiment. We refrain from extracting E_{p} and Γ for the attractive branch for $1/(k_n a) \gtrsim 0.3$.

between $T/T_c \approx 1$ and 4. The width at $T/T_c \approx 1$ shows the same asymmetric dependence on $1/(k_n a)$ as the BEC data [with a maximum at $1/(k_n a) > 0$], but it becomes more symmetric for $T/T_c \approx 4$, with the maximum at $1/(k_n a) \approx 0$. The asymmetry between the attractive and repulsive branches at low T is a many-body effect, due to bound states that exist only for $a > 0$. In the high-T limit, only the two-body scattering states are relevant and the situation for positive and negative a is symmetric.

While the BEC data are well captured by the ideal-polaron theory (solid lines, see also Appendix B), the agreement is only qualitative for the thermal baths; in particular, the experimental widths are about 50% larger than the theoretical ones, and for $T/T_c \approx 1$, the experimental E_p/E_n of the repulsive branch is about 30% larger than the theoretical one.

These differences could arise for at least three reasons: (i) the motion of the impurity induces correlations between bath atoms, which could broaden the spectra, (ii) the ratio of thermal and interaction energy scales is intrinsically different in the ideal-polaron model (where $k_B T_c \approx 0.88 E_n$) and our mobile-impurity case (where $k_B T_c \approx 0.44 E_n$), leading to more significant suppression of (many-body) interaction effects in the theory compared to the experiment; for comparison, in Fig. 2 we also show ideal-polaron FDA calculations at half the bath temperature (dotted lines), so that T/E_n is the same as in the experiment, and (iii) for rf injection starting from a spin-polarized thermal Bose gas, one expects the spectral shifts to be enhanced due to bosonic bunching, which arises from coherence between the impurity and bath states. In the mean-field limit (at low $|a|$), one expects $E_{mf} = 2\pi\hbar^2 \alpha n a/m_r$ with $\alpha = 2$ (compared to $\alpha = 1$ for a pure BEC) [42,43], and such enhancement could still play a role in the strongly interacting regime. However, note that even for low a, we curiously find α closer to 1 (see Appendix C), and understanding the role of coherence in injection experiments remains a challenge for the future.

Finally, we focus on the crossover to the classical Boltzmann-gas regime, in which only two-body effects are relevant and one can (to a good approximation) obtain the spectral shift and width, respectively, from the real and imaginary part of the complex energy $\Sigma = E_p - i\hbar\Gamma = -2\pi\hbar^2 \alpha n f(a)/m_r$, where $f(a) = \langle -a/(1+ika)\rangle_{th}$ is the thermally averaged two-body scattering amplitude (see Appendix D). In this case, the natural interaction parameter is $a/\tilde{\lambda}$, where the mass-adjusted $\tilde{\lambda} = \lambda\sqrt{m/(2m_r)}$ and $\lambda = \sqrt{2\pi\hbar^2/(mk_B T)}$, and the natural energy scale is $E_0 = E_{mf}\tilde{\lambda}/a = 2\pi\hbar^2 \tilde{\lambda} a n/m_r$. Near the resonance, the interactions become unitarity limited: at $\lambda/a = 0$, the scattering amplitude and Σ become purely imaginary, the spectral shift is zero, and the width is maximal.

In Fig. 3, we compare our measurements to this universal high-T prediction (solid line), plotting E_p/E_0 versus $\tilde{\lambda}/a$ for

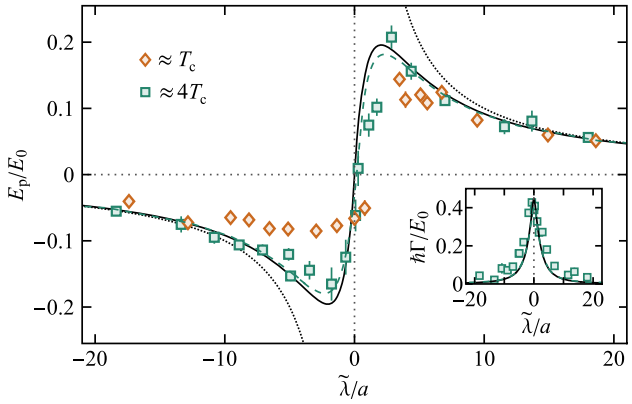


FIG. 3. Crossover to the Boltzmann-gas regime. The main panel shows E_p/E_0 versus $\tilde{\lambda}/a$, where $E_0 = 2\pi\hbar^2\tilde{\lambda} a n/m_r$ and $\tilde{\lambda} = \lambda\sqrt{m/(2m_r)}$. The inset shows $\hbar\Gamma/E_0$ versus $\tilde{\lambda}/a$ for $T/T_c \approx 4$. The solid lines show the universal two-body prediction valid for $T/T_c \gg 1$, while the dotted line shows the mean-field prediction $E_p = E_{mf}$. For reference, the dashed lines show the ideal-polaron theory for $T/T_c = 4$, which for $T \to \infty$ coincides with the universal two-body theory.

our thermal baths; we experimentally determine E_0 from the slope of E_p versus a in the mean-field regime ($|a| \ll \lambda$) (see Appendix C). The E_p data approach the theory for our highest temperature $T/T_c \approx 4$; here the width $\hbar\Gamma/E_0$ also agrees with the theory for $\lambda/a \approx 0$, but is systematically higher away from unitarity (see inset). This temperature corresponds to a phase-space density $n\lambda^3 \approx 0.3$, suggesting that the two-body theory becomes valid only for an essentially nondegenerate bath, while for a degenerate bath near T_c (where all three principal length scales a, λ, and $1/k_n$ are comparable in magnitude) many-body effects are significant [44]. For reference, we show the ideal-polaron theory at $T/T_c = 4$ (dashed lines), which is also already close to the two-body theory (see also Appendix D).

In conclusion, we have investigated the spectral response of impurities strongly interacting with a thermal bosonic bath, revealing the importance of many-body effects in the degenerate regime, and studying the crossover to the classical Boltzmann-gas regime with unitarity-limited scattering. The comparison of our thermal-bath spectra with previous measurements for an impurity in a quasipure BEC highlights the conceptual differences between bosonic and fermionic baths: while sharp quasiparticle features emerge at low T in the fermionic case, the bosonic spectral response is intrinsically broad at strong interactions. The qualitative observations are well captured in the ideal-polaron theory, which neglects impurity motional degrees of freedom and short-range bath correlations, but crucially includes an arbitrary number of bath excitations and can thus capture the macroscopic deformation of the bath.

In the future, it would be interesting to extend our study to the case of light impurities, where Efimov physics is

predicted to play a more important role [46,47], or to systems with stronger intrabath repulsion, where the quasiparticles are expected to be more well defined [13] (see also Refs. [48,49]) and, furthermore, the thermal bath becomes hydrodynamic [50]. It would also be interesting to vary both n and T at different fixed values of T/T_c and to explore impurity concentration effects [51]. Our work motivates the development of novel theoretical approaches that capture the effect of short-range bath correlations [especially relevant for the attractive branch at $1/(k_n a) > 0$] at arbitrary T.

Acknowledgments—We thank Martin Gazo, Richard Schmidt, and Meera Parish for discussions and comments on the manuscript. The Cambridge work was supported by EPSRC (Grants No. EP/P009565/1 and No. EP/Y01510X/1), ERC (UniFlat), and STFC (Grants No. ST/T006056/1 and No. ST/Y004469/1). Z. H. acknowledges support from the Royal Society Wolfson Fellowship. The Heidelberg work was supported by the DFG (German Research Foundation) under Project No. 273811115 (SFB 1225 ISOQUANT) and under Germany's Excellence Strategy EXC2181/1-390900948 (the Heidelberg STRUCTURES Excellence Cluster).

Data availability—The data that support the findings of this article are openly available [52].

[1] L. D. Landau, Electron motion in crystal lattices, Phys. Z. Sowjetunion **3**, 664 (1933).
[2] S. I. Pekar, Autolocalization of the electron in an inertially polarizable dielectric medium, Zh. Eksp. Teor. Fiz. **16**, 335 (1946).
[3] *Polarons in Advanced Materials*, edited by A. S. Alexandrov (Springer, New York, 2008).
[4] C. Franchini, M. Reticcioli, M. Setvin, and U. Diebold, Polarons in materials, Nat. Rev. Mater. **6**, 560 (2021).
[5] F. Scazza, M. Zaccanti, P. Massignan, M. M. Parish, and J. Levinsen, Repulsive Fermi and Bose polarons in quantum gases, Atoms **10**, 55 (2022).
[6] C. Baroni, G. Lamporesi, and M. Zaccanti, Quantum mixtures of ultracold gases of neutral atoms, Nat. Rev. Phys. **6**, 736 (2024).
[7] F. Grusdt, N. Mostaan, E. Demler, and L. A. P. Ardila, Impurities and polarons in bosonic quantum gases: A review on recent progress, Rep. Prog. Phys. **88**, 066401 (2025).
[8] P. Massignan, R. Schmidt, G. E. Astrakharchik, A. İmamoglu, M. Zwierlein, J. J. Arlt, and G. M. Bruun, Polarons in atomic gases and two-dimensional semiconductors, Rev. Mod. Phys. **98**, 035002 (2026).
[9] A. Schirotzek, C.-H. Wu, A. Sommer, and M. W. Zwierlein, Observation of Fermi polarons in a tunable Fermi liquid of ultracold atoms, Phys. Rev. Lett. **102**, 230402 (2009).
[10] C. Kohstall, M. Zaccanti, M. Jag, A. Trenkwalder, P. Massignan, G. M. Bruun, F. Schreck, and R. Grimm, Metastability and coherence of repulsive polarons in a strongly interacting Fermi mixture, Nature (London) **485**, 615 (2012).
[11] Z. Yan, P. B. Patel, B. Mukherjee, R. J. Fletcher, J. Struck, and M. W. Zwierlein, Boiling a unitary Fermi liquid, Phys. Rev. Lett. **122**, 093401 (2019).
[12] S. M. Yoshida, S. Endo, J. Levinsen, and M. M. Parish, Universality of an impurity in a Bose-Einstein condensate, Phys. Rev. X **8**, 011024 (2018).
[13] N.-E. Guenther, R. Schmidt, G. M. Bruun, V. Gurarie, and P. Massignan, Mobile impurity in a Bose-Einstein condensate and the orthogonality catastrophe, Phys. Rev. A **103**, 013317 (2021).
[14] M.-G. Hu, M. J. Van de Graaff, D. Kedar, J. P. Corson, E. A. Cornell, and D. S. Jin, Bose polarons in the strongly interacting regime, Phys. Rev. Lett. **117**, 055301 (2016).
[15] N. B. Jørgensen, L. Wacker, K. T. Skalmstang, M. M. Parish, J. Levinsen, R. S. Christensen, G. M. Bruun, and J. J. Arlt, Observation of attractive and repulsive polarons in a Bose-Einstein condensate, Phys. Rev. Lett. **117**, 055302 (2016).
[16] M. G. Skou, T. G. Skov, N. B. Jørgensen, K. K. Nielsen, A. Camacho-Guardian, T. Pohl, G. M. Bruun, and J. J. Arlt, Non-equilibrium quantum dynamics and formation of the Bose polaron, Nat. Phys. **17**, 731 (2021).
[17] M. G. Skou, K. K. Nielsen, T. G. Skov, A. M. Morgen, N. B. Jørgensen, A. Camacho-Guardian, T. Pohl, G. M. Bruun, and J. J. Arlt, Life and death of the Bose polaron, Phys. Rev. Res. **4**, 043093 (2022).
[18] H. Cayla, P. Massignan, T. Giamarchi, A. Aspect, C. I. Westbrook, and D. Clément, Observation of $1/k^4$-tails after expansion of Bose-Einstein condensates with impurities, Phys. Rev. Lett. **130**, 153401 (2023).
[19] J. Etrych, G. Martirosyan, A. Cao, C. J. Ho, Z. Hadzibabic, and C. Eigen, Universal quantum dynamics of Bose polarons, Phys. Rev. X **15**, 021070 (2025).
[20] R. Schmidt, H. R. Sadeghpour, and E. Demler, Mesoscopic Rydberg impurity in an atomic quantum gas, Phys. Rev. Lett. **116**, 105302 (2016).
[21] N.-E. Guenther, P. Massignan, M. Lewenstein, and G. M. Bruun, Bose polarons at finite temperature and strong coupling, Phys. Rev. Lett. **120**, 050405 (2018).
[22] V. Pastukhov, Polaron in the dilute critical Bose condensate, J. Phys. A **51**, 195003 (2018).
[23] D. Dzsotjan, R. Schmidt, and M. Fleischhauer, Dynamical variational approach to Bose polarons at finite temperatures, Phys. Rev. Lett. **124**, 223401 (2020).
[24] B. Field, J. Levinsen, and M. M. Parish, Fate of the Bose polaron at finite temperature, Phys. Rev. A **101**, 013623 (2020).
[25] G. Pascual and J. Boronat, Quasiparticle nature of the Bose polaron at finite temperature, Phys. Rev. Lett. **127**, 205301 (2021).
[26] M. Drescher, M. Salmhofer, and T. Enss, Bosonic functional determinant approach and its application to polaron spectra, Phys. Rev. A **110**, 063303 (2024).
[27] Z. Z. Yan, Y. Ni, C. Robens, and M. W. Zwierlein, Bose polarons near quantum criticality, Science **368**, 190 (2020).
[28] M. Drescher, M. Salmhofer, and T. Enss, Quench dynamics of the ideal Bose polaron at zero and nonzero temperatures, Phys. Rev. A **103**, 033317 (2021).

[29] R. Schmidt, J. D. Whalen, R. Ding, F. Camargo, G. Woehl, S. Yoshida, J. Burgdörfer, F. B. Dunning, E. Demler, H. R. Sadeghpour, and T. C. Killian, Theory of excitation of Rydberg polarons in an atomic quantum gas, Phys. Rev. A **97**, 022707 (2018).
[30] A. L. Gaunt, T. F. Schmidutz, I. Gotlibovych, R. P. Smith, and Z. Hadzibabic, Bose-Einstein condensation of atoms in a uniform potential, Phys. Rev. Lett. **110**, 200406 (2013).
[31] C. Eigen, A. L. Gaunt, A. Suleymanzade, N. Navon, Z. Hadzibabic, and R. P. Smith, Observation of weak collapse in a Bose–Einstein condensate, Phys. Rev. X **6**, 041058 (2016).
[32] N. Navon, R. P. Smith, and Z. Hadzibabic, Quantum gases in optical boxes, Nat. Phys. **17**, 1334 (2021).
[33] To avoid trapping atoms outside of the optical box, we always start our measurements with a quasipure BEC in a shallow trap of depth $U_D \approx k_B \times 50$ nK. We then raise the depth to $U_D \approx k_B \times 1$ μK, inject energy by sinusoidally forcing the system using a magnetic-field gradient, and allow the gas to rethermalize at $a_b \approx 100 a_0$.
[34] To minimize Fourier broadening and stay in the linear-response regime, here we use pulse durations $t_{rf} = \{0.8\text{–}6.4\}$ ms and always limit the injection fractions to $\lesssim 10\%$.
[35] Note that in the ideal-polaron theory, the spectra are expected to evolve continuously as the bath temperature is increased, with no sharp change at T_c, and we have experimentally checked that the injection spectra do not qualitatively change just below T_c.
[36] Y. E. Shchadilova, R. Schmidt, F. Grusdt, and E. Demler, Quantum dynamics of ultracold Bose polarons, Phys. Rev. Lett. **117**, 113002 (2016).
[37] J. Levinsen, L. A. Peña Ardila, S. M. Yoshida, and M. M. Parish, Quantum behavior of a heavy impurity strongly coupled to a Bose gas, Phys. Rev. Lett. **127**, 033401 (2021).
[38] A. Y. Chuang, H. Q. Bui, A. Christianen, Y. Zhang, Y. Ni, D. Ahmed-Braun, C. Robens, and M. Zwierlein, Observation of a halo trimer in an ultracold Bose–Fermi mixture, Phys. Rev. X **15**, 021098 (2025).
[39] C. Robens, A. Christianen, A. Y. Chuang, H. Q. Bui, Y. Zhang, R. Schmidt, and M. Zwierlein, Polaronic hybridization of atoms, dimers and trimers in a Bose-Einstein condensate, arXiv:2606.20440.
[40] B. Mukherjee, P. B. Patel, Z. Yan, R. J. Fletcher, J. Struck, and M. W. Zwierlein, Spectral response and contact of the unitary Fermi gas, Phys. Rev. Lett. **122**, 203402 (2019).
[41] We always correct Γ for residual Fourier broadening arising from our finite rf-pulse times, t_{rf}, using $\Gamma = (\Gamma_e^2 - \Gamma_t^2)^{1/2}$, where Γ_e is the raw extracted width and $\Gamma_t \approx 2.78/t_{rf}$ is the width of our response function [19].
[42] D. M. Harber, H. J. Lewandowski, J. M. McGuirk, and E. A. Cornell, Effect of cold collisions on spin coherence and resonance shifts in a magnetically trapped ultracold gas, Phys. Rev. A **66**, 053616 (2002).
[43] M. W. Zwierlein, Z. Hadzibabic, S. Gupta, and W. Ketterle, Spectroscopic insensitivity to cold collisions in a two-state mixture of fermions, Phys. Rev. Lett. **91**, 250404 (2003).
[44] Note that similar conclusions were obtained in interferometric experiments with single-component Bose gases [45]; for $n\lambda^3 = 0.13$ ($T/T_c \approx 7$) the measurements were consistent with the two-body theory, but measurements for $n\lambda^3 = 0.54$ ($T/T_c \approx 3$) revealed effects of three-body correlations.
[45] R. J. Fletcher, R. Lopes, J. Man, N. Navon, R. P. Smith, M. W. Zwierlein, and Z. Hadzibabic, Two- and three-body contacts in the unitary Bose gas, Science **355**, 377 (2017).
[46] M. Sun, H. Zhai, and X. Cui, Visualizing the Efimov correlation in Bose polarons, Phys. Rev. Lett. **119**, 013401 (2017).
[47] A. Christianen, J. I. Cirac, and R. Schmidt, Phase diagram for strong-coupling Bose polarons, SciPost Phys. **16**, 067 (2024).
[48] R. Henke, J. Levinsen, M. M. Parish, J. Boronat, G. E. Astrakharchik, H. Moritz, and C. R. Cabrera, Realization of repulsive polarons in the strongly correlated regime, Phys. Rev. X (2026).
[49] R. Alhyder, G. M. Bruun, T. Pohl, M. Lemeshko, and A. G. Volosniev, Phenomenological model of decaying Bose polarons, Phys. Rev. Res. **8**, L012034 (2026).
[50] T. A. Hilker, L. H. Dogra, C. Eigen, J. A. P. Glidden, R. P. Smith, and Z. Hadzibabic, First and second sound in a compressible 3D Bose fluid, Phys. Rev. Lett. **128**, 223601 (2022).
[51] C. Baroni, B. Huang, I. Fritsche, E. Dobler, G. Anich, E. Kirilov, R. Grimm, M. A. Bastarrachea-Magnani, P. Massignan, and G. M. Bruun, Mediated interactions between Fermi polarons and the role of impurity quantum statistics, Nat. Phys. **20**, 68 (2024).
[52] J. Etrych, S. J. Morris, S. M. Fischer, G. Martirosyan, C. J. Ho, M. Drescher, M. Salmhofer, Z. Hadzibabic, T. Enss, and C. Eigen, Research data supporting "Fate of an impurity strongly interacting with a thermal Bose gas" (2026), 10.17863/CAM.134561.
[53] M. Drescher, M. Salmhofer, and T. Enss, Theory of a resonantly interacting impurity in a Bose-Einstein condensate, Phys. Rev. Res. **2**, 032011(R) (2020).
[54] R. Lopes, C. Eigen, N. Navon, D. Clément, R. P. Smith, and Z. Hadzibabic, Quantum depletion of a homogeneous Bose-Einstein condensate, Phys. Rev. Lett. **119**, 190404 (2017).

End Matter

Appendix A: Functional determinant approach—Following Refs. [26,28,53] (see also Refs. [23,29]), for a mobile equal-mass impurity in a Bose gas, one can write the Hamiltonian in the frame comoving with the impurity as

$$\hat{H} = \sum_i \frac{\hat{\mathbf{p}}_i^2}{2m_r} + \sum_i V_{IB}(\hat{\mathbf{x}}_i) + \frac{:(\sum_i \hat{\mathbf{p}}_i - \mathbf{p}_0)^2:}{2m}, \quad \text{(A1)}$$

where $\mathbf{p}_0$ is the impurity momentum, $\hat{\mathbf{p}}_i$ and $\hat{\mathbf{x}}_i$ denote the momentum and position operators of the ith bath

boson, and V_{IB} is the impurity-boson potential centered around $\mathbf{x} = 0$ in the comoving frame. The third term on the rhs accounts for impurity recoil and generates effective higher-order correlations between bath particles; $:\cdots:$ denotes normal ordering. Throughout, we set this third term to zero; note that this approximation is exact in the high-temperature, two-body, and weak-interactions limits. The real-time response of the system is then given by

$$S(t) = \langle e^{i\hat{H}_0 t/\hbar} e^{-i\hat{H}t/\hbar} \rangle, \tag{A2}$$

where $\hat{H}_0$ denotes the Hamiltonian with $V_{\mathrm{IB}} = 0$. This response has contributions from the condensate that is present for $T < T_c$, from the thermal modes for $T > 0$, and from the correlations between condensate and thermal modes for $0 < T < T_c$; see Ref. [26] for the explicit expressions. Finally, the measured rf spectrum is obtained as the Fourier transform

$$I(\delta) = \frac{1}{\pi} \mathrm{Re} \int_0^\infty S(t) e^{i\delta t} \mathrm{d}t. \tag{A3}$$

Appendix B: Effect of nonzero T for impurities in a BEC—In Fig. 4, we illustrate the effect of a small nonzero T in the theory (see also Ref. [26]). We plot the ideal-polaron theory for $T = 0$ and for different small T/T_c, alongside our BEC data. The theoretical E_p values for the repulsive branch show only small variation with T, while $|E_p|$ of the attractive branch for $-1 \lesssim 1/(k_n a) \lesssim 0$ is suppressed with increasing T. For $1/(k_n|a|) \gtrsim 1$, the theoretical Γ is very small only for $T = 0$, and any small T causes significant broadening. On the other hand, near $1/(k_n a) \approx 0$, Γ changes only slowly with T. We find that $T/T_c = 0.15$ captures the data reasonably well for all $1/(k_n a)$.

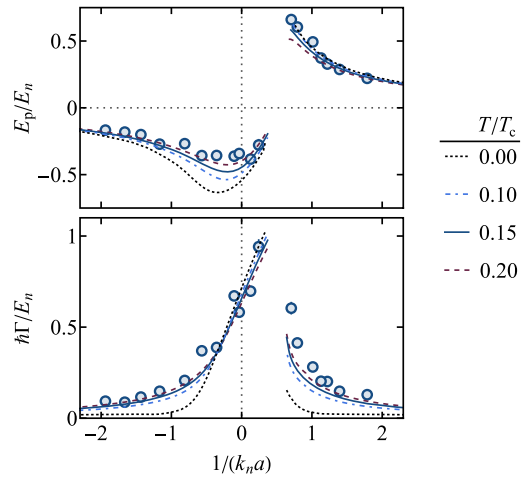


FIG. 4. Comparison of our BEC-bath data [19] with the ideal-polaron theory at zero and nonzero T. Plot of E_p/E_n (top) and $\hbar\Gamma/E_n$ (bottom) versus $1/(k_n a)$, showing the data (symbols) and the ideal-polaron theory at different T/T_c (legend).

Initially, our quasipure BEC has $T \approx 10$ nK [54] such that $T/T_c < 0.1$, but both the impurities and the bath can be excited during injection, due to dynamics arising from inhomogeneity near the box edges and due to three-body losses. The effect of such excitations should be captured by an elevated (effective) T, and for the theory comparisons in Figs. 1 and 2 we used $T/T_c = 0.15$.

Appendix C: Spectral shifts in the weakly interacting regime—In Fig. 5, we show our measured E_p values for low $|a|$, where spectral shifts reflect the mean-field impurity energy $E_{\mathrm{mf}} = 2\pi\hbar^2 \alpha n a / m_r$. For our BEC data [19], we used such measurements to calibrate the bath density. Here, for our thermal baths, we directly obtain the bath atom number N and temperature T from time-of-flight absorption images, and calculate the density using the independently measured V [30].

For injection spectroscopy of a thermal gas, one expects $\alpha = 2$, reflecting the enhanced probability of finding two identical bosons on top of each other in the initial single-component gas [42,43]; for a BEC, on the other hand, $\alpha = 1$. However, fitting our data in Fig. 5 gives $\alpha = 1.1(4)$, with the error dominated by our systematic uncertainties in N and V. Experimentally, the measured α should be slightly lower than 2 due to the nonzero fraction of transferred impurities, but since our transfer fractions are $\lesssim 10\%$, this explains only a small part of the discrepancy.

Appendix D: Two-body theory valid for $T/T_c \gg 1$—In the high-T limit, for any impurity mass, the ideal-polaron theory coincides with the universal two-body theory, which gives the spectral shift and width,

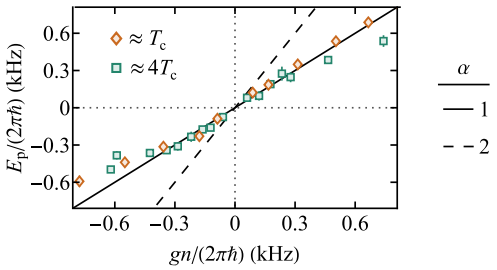


FIG. 5. Mean-field energy shift in the weakly interacting regime. Spectrum mode E_p versus gn, where $g = 2\pi\hbar^2 a/m_r$. The solid and dashed lines show $E_p = \alpha g n$ with, respectively, $\alpha = 1$ and 2 (see text for details).

respectively, from the real and imaginary parts of the complex energy $\Sigma = E_{\mathrm{p}} - i\hbar\Gamma = -2\pi\hbar^2\alpha n f(a)/m_{\mathrm{r}}$, where

$$f(a) = -\frac{\tilde{\lambda}^3}{2^{3/2}\pi^3}\int \frac{a}{1+ika}\exp\left(-\frac{\hbar^2k^2}{2m_{\mathrm{r}}k_{\mathrm{B}}T}\right)\mathrm{d}^3k \tag{D1}$$

is the thermally averaged scattering amplitude. More explicitly, one obtains the universal functions:

$$\frac{E_{\mathrm{p}}}{E_0} = \frac{v}{\pi}\left[1 - \frac{|v|}{\sqrt{2}}\exp\left(\frac{v^2}{2\pi}\right)\mathrm{erfc}\left(\frac{|v|}{\sqrt{2\pi}}\right)\right], \tag{D2}$$

$$\frac{\hbar\Gamma}{E_0} = \frac{\sqrt{2}}{\pi}\left[1 + \frac{v^2}{2\pi}\exp\left(\frac{v^2}{2\pi}\right)\mathrm{Ei}\left(\frac{-v^2}{2\pi}\right)\right], \tag{D3}$$

where $v = \tilde{\lambda}/a$ and $\mathrm{Ei}(x)$ denotes the exponential integral.